Published in final edited form as:
Cancer Cell. 2011 May 17; 19(5): 629–639. doi:10.1016/j.ccr.2011.03.023.

PTPN11/Shp2 Acts as a Tumor Suppressor in Hepatocellular Carcinogenesis

Emilie A. Bard-Chapeau[1,2,#], **Shuangwei Li**[1,#], **Jin Ding**[3], **Sharon S. Zhang**[1], **Helen H. Zhu**[1], **Frederic Princen**[2], **Diane D. Fang**[1], **Tao Han**[3], **Beatrice Bailly-Maitre**[2], **Valeria Poli**[4], **Nissi M. Varki**[1], **Hongyang Wang**[3], and **Gen-Sheng Feng**[1,2,3,*]

[1]Department of Pathology, and Division of Biological Sciences, University of California San Diego, La Jolla, California 92093-0864

[2]Sanford/Burnham Medical Research Institute, La Jolla, California 92037

[3]Laboratory of Signal Transduction, Eastern Hepatobiliary Surgery Hospital, Second Military Medical University, Shanghai, China 200433

[4]Department of Genetics, Biology, and Biochemistry, University of Turin, Turin, Italy

SUMMARY

The human gene *PTPN11*, which encodes the tyrosine phosphatase Shp2, may act as a proto-oncogene, as dominantly activating mutations have been detected in several types of leukemia. Herein we report a tumor suppressor function of Shp2. Hepatocyte-specific deletion of Shp2 promotes inflammatory signaling through the Stat3 pathway and hepatic inflammation/necrosis, resulting in regenerative hyperplasia and development of tumors in aged mice. Furthermore, Shp2 ablation dramatically enhanced diethylenenitrite (DEN)-induced hepatocellular carcinoma (HCC) development, which was abolished by concurrent deletion of Shp2 and Stat3 in hepatocytes. Decreased Shp2 expression was detected in a sub-fraction of human HCC specimens. Thus, in contrast to the leukemogenic effect of dominant active mutants, *PTPN11/Shp2* has a tumor suppressor function in liver.

INTRODUCTION

The advancement in understanding the molecular basis of carcinogenesis has benefited tremendously from genetic and functional analyses of oncogenes and tumor suppressor genes (Levine and Puzio-Kuter, 2010; Weinberg, 1995). In conventional view, the genesis of cancer can be triggered by dominant, gain of function, mutations in proto-oncogenes and recessive, loss of function, mutations in tumor suppressor genes or anti-oncogenes (Bishop, 1991). Studies initiated on *v-Src* and *c-Src* have revealed essential roles of tyrosine kinases in regulation of cell proliferation, and their oncogenic activation in promoting malignant transformation (Blume-Jensen and Hunter, 2001; Sefton and Hunter, 1986). This conception has naturally predicted tyrosine phosphatases functioning as tumor suppressors. Indeed, genetic data have implicated loss or inactivation of tyrosine phosphatase genes in cancer

*To whom the correspondence should be addressed: Dr. Gen-Sheng Feng, Tel: (858) 822-5441; Fax: (858) 822-1966, gfeng@ucsd.edu.
#These two authors contributed equally to this work

The authors declare no conflict of interest.

development and metastasis (Revillion et al., 2009; Sun et al., 2011; Veeriah et al., 2009; Wang et al., 2004).

Interestingly, recent work has led to identification of *PTPN11*/*Shp2* as a proto-oncogene (Chan and Feng, 2007; Tartaglia et al., 2003). Shp2 is an intracellular tyrosine phosphatase with two Src-homology 2 (SH2) domains that acts to promote activation of the Ras-Erk pathway by growth factors, cytokines and hormones (Lai et al., 2004; Neel et al., 2003). Autosomal dominant mutations in the human gene *PTPN11* have been detected in nearly 50% of Noonan syndrome patients who have higher risk of suffering juvenile myelomonocytic leukemia (JMML), and somatic mutations constitutively activating Shp2 have also been found in several types of leukemia (Tartaglia and Gelb, 2005). Overexpression of Shp2 was detected in leukemia and breast cancer cell lines and patient samples (Xu et al., 2005; Zhou et al., 2008). In previous work, we generated a hepatocyte-specific Shp2 knockout ($Shp2^{hep-/-}$) mouse model, and found that Shp2 deletion suppressed Erk signal and hepatocyte proliferation following partial hepatectomy (Bard-Chapeau et al., 2006). The effect of Shp2 in amplification of proliferative signal in hepatocytes is consistent with a body of literature documenting a positive role of this phosphatase in cellular responses to mitogenic stimuli (Lai et al., 2004; Neel et al., 2003).

The present study is designed to investigate the possible tumor suppressor function of *PTPN11/Shp2* in liver.

RESULTS

$Shp2^{hep-/-}$ mice developed hepatic inflammation and necrosis

Shp2 was deleted in hepatocytes in $Shp2^{hep-/-}$ mice that were generated by crossing $Shp2^{flox/flox}$ mice with *Albumin-Cre* transgenic mice (Bard-Chapeau et al., 2006). $Shp2^{hep-/-}$ mice were born with the expected frequency and morphologically indistinguishable from their control littermates. The body weights were similar between $Shp2^{hep-/-}$ and control animals at 2-month of age in fed or fasting state (Figure S1A). There was also no difference between control and $Shp2^{hep-/-}$ young mice in the ratio of liver weight to body weight (Figure S1B). Serum levels of alanine aminotransferase (ALT) and aspartate aminotransferase (AST) were significantly higher in $Shp2^{hep-/-}$ mice than that in controls (Figure 1A). Macroscopic examination revealed one or several foci of pallor noticeable on the liver surface in 34% of dissected $Shp2^{hep-/-}$ animals (n=21) (Figure 1B). Hematoxylin and eosin (H&E) staining of liver sections showed large areas of parenchymal necrosis (Figure 1C). Smaller focal areas of parenchymal necrosis were also detected (Figure 1D, 1E). Necrosis was observed in 47% of $Shp2^{hep-/-}$ animals (n=21) in contrast to 0% of control mice (n=11). TUNEL assay revealed no significant difference in apoptosis between control and $Shp2^{hep-/-}$ livers (data not shown). A large proportion (93%) of $Shp2^{hep-/-}$ livers (n=21) contained areas with infiltrate of inflammatory cells (Figure 1D–1F), which appeared to concentrate around the portal triads with extension into the parenchyma. Inflammatory cells were visible outside, around or inside the necrotic areas. Necrotic zones were always associated with inflammatory cells (Figure 1C–E), whereas inflammation was occasionally observed without necrosis (Figure 1F). Signs of fibrosis were found at the portal triads, but not near the necrosis or into parenchyma, as revealed by trichrome staining (Figure 1G, 1H).

We detected significantly increased amounts of circulating IL-6 in $Shp2^{hep-/-}$ animals, among 11 cytokines examined (Figure 1I). We then examined local expression of cytokine and inflammatory genes in the liver by real-time RT-PCR (Figure 1J). Hepatic expression of *IL-6, TNFα* and *SAP (serum amyloid-P)* mRNAs was remarkably elevated in $Shp2^{hep-/-}$

livers, while transcripts of *hepatocyte growth factor (HGF)* and *Bcl-xl* were not changed (Figure 1J).

Enhanced hepatic and systemic inflammatory responses to LPS in $Shp2^{hep-/-}$ animals

To define hepatic inflammatory responses in $Shp2^{hep-/-}$ mice, we assessed induction of liver damage by lipopolysaccharides (LPS) challenge. Intraperitoneal LPS injection elicited a stronger liver damage response in $Shp2^{hep-/-}$ mice than in controls, as indicated by higher serum ALT levels (Figure 2A). We also measured the ratio of spleen versus body weight, to assess systemic inflammatory response. $Shp2^{hep-/-}$ animals displayed an increase of 130% in their spleen size 14 days after LPS challenge as compared to 98% for control animals (Figure 2B), suggesting an aggravated immune/inflammatory response when Shp2 was removed in hepatocytes. H&E staining of liver sections also revealed increased inflammatory cell infiltration into hepatic parenchyma (Figure 2C).

We measured circulating levels of inflammatory cytokines at different time points following LPS injection (Figure 2D, 2E), and detected similarly increased levels for IFNγ, RANTES, IL-12, IL-1β and IL-10 in control and $Shp2^{hep-/-}$ mice (Figure 2E). However, higher levels of IL-6 and TNF were detected in $Shp2^{hep-/-}$ than in control mice after LPS injection, suggesting an enhanced IL-6 production in $Shp2^{hep-/-}$ animals (Figure 2D).

Shp2 deficiency in hepatocytes leads to enhanced inflammatory signaling in the liver

To dissect intracellular signaling events, we prepared liver extracts after LPS injection into vena cava for 5 min, or intraperitoneally for longer time periods. LPS-stimulated pY-Stat3 and pY-Stat1 signals were increased and prolonged in $Shp2^{hep-/-}$ liver compared to control (Figure 3A, 3B). Degradation of Iκ Bα was potentiated at 1 hr after LPS challenge, p-Erk1/2 and p-p38 signals were impaired, while p-Jnk1/2 levels were elevated at 1 and 3 hrs in mutant samples (Figure 3A, 3B).

To directly evaluate IL-6 signaling in the liver, we injected recombinant IL-6 through the portal vein (Figure 3C). $Shp2^{hep-/-}$ livers responded more potently than controls in induction of pY-Stat3 and pY-Stat1 signals. Quantitative analysis of 4 mice in each genotype revealed a 2.1 fold increase of IL-6-induced pY-Stat3 signal in $Shp2^{hep-/-}$ livers over controls. In contrast, Shp2 deletion suppressed Erk activation by IL-6, indicating a unique negative role of Shp2 in regulating the IL-6/Stat3 pathway in the liver.

Shp2 removal promotes inflammatory signaling through Stat3 in hepatocytes

The hepatic inflammatory response involves communication of different cell types such as hepatocytes and Kupffer cells. In $Shp2^{hep-/-}$ mice, *Shp2/Ptpn11* was deleted in hepatocytes only, due to cell type-specific *Cre* expression directed by the *Albumin* promoter. To determine the cell-intrinsic effect of Shp2 ablation, we isolated primary hepatocytes for treatment with LPS (5 μg/ml) in vitro. As shown in Figure 3D, Shp2 deletion had no effect on LPS stimulation of IκBα degradation (hence NF-κB activaton) in hepatocytes. However, LPS-induced pY-Stat3 signal was enhanced and prolonged in Shp2-deficient hepatocytes. LPS-stimulated p-Erk and p-p38 signals were impaired, while p-Jnk levels were elevated in mutant, compared to control cells (Figure 3D). Akt was mildly stimulated by LPS in hepatocytes with higher basal and activated levels detected in mutants. Thus, Shp2 acts as a negative regulator for Stat3, Jnk and Akt, while positively modulating Erk and p38 induction in hepatocytes by LPS (Figure 3D).

Consistently, pY-Stat3 signal was enhanced and sustained in $Shp2^{-/-}$ hepatocytes following IL-6 treatment, whereas no significant change was detected for Stat1. IL-6-induced p-Erk and p-p38 levels were reduced, and p-Akt signal was elevated in mutant cells compared to

controls (Figure 3E). We simultaneously measured LPS-induced cytokine secretion by hepatocytes in the culture medium (Figure 3F). LPS stimulation caused higher IL-6 secretion by Shp2-deficient hepatocytes, while comparable secretion levels were observed in control and mutant hepatocytes for several other cytokines, with mild increase of IL-12 and IL-10 detected at 24 hrs of LPS stimulation (Figure 3G).

Shp2 ablation leads to development of hepatocellular tumor in aged animals

We followed *Shp2*$^{hep-/-}$ mice longitudinally to assess their phenotype later in life, and detected efficient Shp2 deletion at 1 year of age (Figure 4A). Aged *Shp2*$^{hep-/-}$ mice became leaner by 10.7% for male and 14.9% for female mice, with a significant decrease of their body weights at 1-year (Figure S2A), although their livers were at normal size (Figure S2B). Beginning at 5 month of age, microscopic foci resembling regenerative foci were noticeable in the liver of *Shp2*$^{hep-/-}$ animals. Nodular regenerative hyperplasia was detected in *Shp2*$^{hep-/-}$ animals from 8 months of age. At 12–18 months of age, one or a few spherical macroscopic adenomas measuring 0.1–1 cm in diameter were frequently detected in *Shp2*$^{hep-/-}$ mice (13/19) under both capsular and cut surface, which was not detectable in control animals (0/16). The tumors bulged from the liver surface and were often paler than the hepatic parenchyma (Figure 4B), but sometimes darker or red when accompanied by bleeding. On liver sections, the tumors were unencapsulated, quite well delimited, showing expanding masses of hepatocytes, and positively stained with reticulin (Figure 4C).

The development of hepatocellular adenoma suggests increased and neoplastic proliferation of hepatocytes in the absence of Shp2, and we performed bromodeoxyuridine (BrdU) incorporation assay to quantify cell proliferation rate. BrdU^{+} hepatocyte number was increased in *Shp2*$^{hep-/-}$ animals as compared to littermate controls (Figure 4D). We found an average of 7.8% BrdU^{+} cells in control animals (n=5) versus 25.4% in the abnormal tissue of *Shp2*$^{hep-/-}$ animals (n=10), a significant increase of hepatocyte proliferation. Histological analysis of hepatic parenchyma revealed signs of regenerative hyperplasia with 13 of 19 *Shp2*$^{hep-/-}$ livers having nodule formation (Figure 4E–4G). In most cases, the lobular architecture was distorted by the development of hyperplastic hepatocyte plates (Figure 4E–G). The space between hepatocytes was strikingly reduced inside the nodules (Figure 4E). TUNEL assay performed on liver sections revealed low number of apoptotic hepatocytes in *Shp2*$^{hep-/-}$ liver parenchyma (Figure 4H). However, inside of or surrounding the hyperplastic nodules, massive hepatocyte degeneration was usually found, in association with vacuoles containing eosinophilic material (Figure 4G–H). This explains the high levels of serum ALT and AST in 12–18 month-old *Shp2*$^{hep-/-}$ mice despite the absence of hepatic necrosis at that age (Figure 1A). Although parenchymal necrosis and inflammation were not detected, aged mutant animals presented focal microgranuloma (8/19) consisting of mononuclear inflammatory cells (Figure 4E). To determine altered signaling events underlying development of hepatic adenoma in aged *Shp2*$^{hep-/-}$ animals, we evaluated the activation status of several signaling molecules (Figure 4I). Elevated tyrosine phosphorylation levels of Stat3 were detected in 2 of 4 tumor samples. Efficient Shp2 deletion was steadily detected in adenoma cells suggesting that escaped deletion of *Shp2*$^{flox/flox}$ cells was not the cause of adenoma development/progression in *Shp2*$^{hep-/-}$ mice (Figure 4I).

To explore the possible tumor-suppressing role of Shp2 in human hepatocellular carcinoma (HCC) development, we screened 104 HCC specimens for Shp2 expression and detected dramatically decreased Shp2 protein levels in HCC in 12 samples, as compared to their surrounding tissue (Figure 4J). This observation suggests that Shp2 deficiency is likely one of the molecular mechanisms underlying initiation and/or progression of some human HCCs.

Stat3 is required for promotion of HCC development by Shp2 deletion

To further determine the anti-oncogenic action of Shp2 in liver malignancy, we evaluated the effect of Shp2 removal on HCC in mice induced by chemical carcinogen. Control and $Shp2^{hep-/-}$ mice were injected with a single dose of diethylnitrosamine (DEN) on postnatal day 15, and animals were dissected after 8 months to examine HCC incidences, as described previously (He et al., 2010; Maeda et al., 2005). All the male animals in both control and $Shp2^{hep-/-}$ groups developed visible hepatic tumor foci (Figure 5A). However, hepatocyte-specific deletion of Shp2 dramatically increased the number and sizes of liver tumors (Figure 5A–5C). We also used liver/body weight ratio to determine the tumor burden in DEN-treated animals. As shown in Figure 5D, the ratio increased almost one fold in $Shp2^{hep-/-}$ animals, compared to controls. Consistent with the observation of spontaneous tumor development in aged $Shp2^{hep-/-}$ mice, these results strongly support a notion that Shp2 is a tumor suppressor in HCCs elicited by chemical carcinogen.

We detected elevated pY-Stat3 levels in most of the tumor and surrounding tissues in $Shp2^{hep-/-}$ livers, as compared to controls (Figure 5F), suggesting constitutive activation of the Stat3 pathway in HCCs devoid of Shp2. This observation is also consistent to results shown in Figure 3 that Shp2 removal resulted in enhanced inflammatory signaling through Stat3. To determine the role of Stat3 in hepatocarcinogenesis enhanced by Shp2 deficiency, we generated hepatocyte-specific Shp2/Stat3 double knockout (DKO) mice and examined DEN-induced HCCs. Interestingly, simultaneous deletion of Shp2 and Stat3 in hepatocytes significantly suppressed the promoting effect of Shp2 ablation on HCC development (Figure 5A–5E). Although the tumor frequency and sizes were still higher in DKO than in control animals, there was no difference between DKO and $Stat3^{hep-/-}$ male mice. This data indicates that concurrent removal of Stat3 and Shp2 abolishes completely the impact of Shp2 deficiency on HCC, as the tumor occurrence in DKO mice represented the effect elicited by Stat3 ablation alone. Similar results were obtained in female animals (Figure 5E), over 70% of $Shp2^{hep-/-}$ female mice developed visible foci, 6 fold higher than controls; the tumor incidence was reduced by 50% in DKO and $Stat3^{hep-/-}$ female mice. Of note, PCR analysis of genomic DNA and immunoblot analysis of protein contents confirmed efficient deletion of Shp2 and/or Stat3 in tumors and normal hepatic tissues in respective animals (Figure 5G, 5H), as genotyped by PCR analysis of tail DNA. In aggregate, these results show that Shp2 removal exacerbates DEN-induced HCC development, which requires Stat3. However, deletion of Stat3 in hepatocytes did not prevent HCC occurrence, in contrast to a previous report (He et al., 2010).

Tumors from both control and $Stat3^{hep-/-}$ livers showed typical trabecular structure of HCC (Figure 6A and 6D). However, tumors from $Shp2^{hep-/-}$ and DKO livers lost the trabecular architecture. Infiltrate of inflammatory cells was visible in the portal triads of $Shp2^{hep-/-}$ and DKO livers (Figure 6F and 6G), but rarely observed in *WT* and $Stat3^{hep-/-}$ portal triads. These tumors also displayed eosin-positive cytoplasmic inclusions (Figure 6B and 6C); and the inclusions in DKO tumors were much smaller (Figure 6C). H&E staining of liver tissues showed evident fat droplets in $Stat3^{hep-/-}$ livers. Both $Shp2^{hep-/-}$ and DKO animals exhibited significantly higher levels of serum ALT than controls, but ALT levels were lower in DKO animals than in $Shp2^{hep-/-}$ animals (Figure 6I). We also checked the hepatic inflammatory cytokines TNF and IL-6, and levels of both cytokines were increased in $Shp2^{hep-/-}$ livers, which was abolished by additional deletion of Stat3 (Figure 6J–K). This result was confirmed by qRT-PCR of *IL-6* and *TNFα* transcripts (Figure 6L–M).

DISCUSSION

The results presented here indicate that selective deletion of *Ptpn11/Shp2* in hepatocytes caused hepatic inflammation and necrosis, leading to nodular regenerative hyperplasia. The

enhanced inflammatory signaling may have promoted liver tumorigenesis, resulting in dramatic increase of both spontaneous tumors and DEN-induced HCCs in *Shp2*$^{hep-/-}$ mice. Consistent to the data obtained in the animal model, we also detected deficient/reduced Shp2 expression in 11.5% human HCC samples. It will be interesting to determine whether there are deletion or point mutations at the *PTPN11/Shp2* locus in HCC genomes that could result in functional inactivation of this tyrosine phosphatase.

The tumor-suppressing role of *PTPN11/Shp2* in HCC is unexpected, as our previous experiments indicated a positive role of Shp2 in regulation of hepatocyte proliferation and growth factor signaling through the Ras-Erk pathway by working in concert with Gab1 adaptor protein (Bard-Chapeau et al., 2006). Furthermore, inherited or somatic mutations in human *PTPN11/Shp2* gene have been implicated in Noonan syndrome or several types of leukemia, particularly JMML, thus identifying *PTPN11* as a proto-oncogene (Chan and Feng, 2007; Tartaglia et al., 2006). However, the inhibitory role of Shp2 on liver cancer is very similar to the dual function of the IKK/NF-κB pathway. Karin's group demonstrated an inhibitory effect of IKKβ/NF-κB pathway on DEN-induced HCC development (Maeda et al., 2005), in contrast to its tumor-promoting effect in colitis-associated cancer (CAC) (Greten et al., 2004). Deletion of NEMO/IKK also resulted in spontaneous development of hepatocellular carcinoma in mice (Luedde et al., 2007). He et al. demonstrated further that deletion of IKKβ in hepatocytes promoted HCC progression through upregulation of reactive oxidative stress (ROS) (He et al., 2010).

Rapidly growing evidence reinforces the notion that tumors are promoted by inflammatory signals in the surrounding microenvironment (Coussens and Werb, 2002; Yu et al., 2007). In this report, we show that hepatocyte-specific deletion of Shp2 resulted in marked increase of the inflammatory IL-6/Stat3 signal strength. Consistent to this observation is the previous work documented by us and others on a negative regulatory role of Shp2 in Jak-Stat signaling (Bard-Chapeau et al., 2006; Chan et al., 2003; Servidei et al., 1998; Wu et al., 2009; You et al., 1999). Of note, we found that Shp2 ablation, while promoting IL-6-stimulated Stat3 activation, had no effect on IκBα degradation (NF-κB activation), suggesting that Shp2 acts downstream of, or in parallel with, NF-κB in modulation of Stat3 activity.

Indeed, a critical role of Stat3 in mediating inflammation-provoked malignancy has been reported in several types of cancer (Yu et al., 2009). To address the requirement for Stat3 in liver cancer elicited or enhanced by Shp2 ablation, we generated hepatocyte-specific Shp2/Stat3 DKO mice. Combined deletion of both Shp2 and Stat3 in hepatocytes completely alleviated the effect of Shp2 loss on HCC development, supporting our theory that augmented Stat3 activation plays an essential role in hepatocarcinogenesis in *Shp2*$^{hep-/-}$ mice. However, it is also interesting to note that deletion of Stat3 in hepatocytes did not prevent HCC development in the DEN-induced mouse tumor model. In fact, Stat3 removal caused a modest but statistically significant increase in DEN-induced HCC number and sizes, compared to wild-type controls. This unexpected observation of enhanced HCC development in *Stat3*$^{hep-/-}$ mice indicates complexity of molecular mechanisms underlying liver malignancy. A body of literature documented constitutive or enhanced activation of Stat3 in different types of cancer (He et al., 2010; Yu et al., 2009). It will be interesting to determine why and how Stat3 deletion also exacerbates hepatocarcinogenesis.

Since tumor incidence was increased in both *Shp2*$^{hep-/-}$ and *Stat3*$^{hep-/-}$ mice, one would expect to observe an additive or synergistic effect on HCC by simultaneous deletion of Shp2 and Stat3, i.e. even more severe tumor development in DKO mice. In contrast, we observed alleviation of the Shp2 deletion effect by Stat3 removal, which indicates a distinct mechanism of liver cancer in *Stat3*$^{hep-/-}$ mice. Despite a requirement of Stat3 for

aggravated HCC development induced by Shp2 deficiency, Stat3 is evidently unnecessary for liver malignancy in this animal model. Although the mechanism for HCC development induced by Stat3 deficiency is unknown, results presented here suggest that Shp2 presence or absence does not have any influence on HCC development enhanced by Stat3 removal. Elucidating the paradoxical roles of Shp2 and Stat3, as well as several other molecules, acting as either tumor promoter or suppressor will shed lights on molecular basis of cancer and may suggest therapeutic strategies for the malignant diseases.

EXPERIMENTAL PROCEDURES

Mice and liver tumorigenesis

Hepatocyte-specific Shp2 knockout (*Shp2*$^{hep-/-}$, previously called LSKO, liver-specific Shp2 knockout) mice (C57BL/6) were generated as previously described (Bard-Chapeau et al., 2006). *Shp2*$^{flox/flox}$ littermates were used as control mice. Genotyping was done by PCR analysis on genomic DNA extracted from mouse tails (Bard-Chapeau et al., 2006; Zhang et al., 2004). *Stat3*^{flox} mice were reported previously (Alonzi et al., 2001). Hepatocyte-specific Shp2/Stat3 double KO mice were generated by crossing *Shp2*$^{hep-/-}$ (*Shp2*$^{flox/flox}$*:Alb-Cre*) with *Stat3*$^{flox/flox}$ mice. Genotyping of the *Stat3*^{flox} allele was done by PCR analysis on tail genomic DNA using a pair of primers (forward 5’-CAC CAA CAC ATG CTA TTT GTA GG-3’ and reverse 5’CCT GTC TCT GAC AGG CCA TC-3’). To determine Stat3 deletion in hepatocytes, genomic DNA was extracted from liver using NucleaoSpin Tissue Kit. PCR was done using a pair of primers (forward 1: 5’-AGA GAG CGT CTG ACT CTA CAA CCC T-3’; forward 2: 5’-GGG ATG TTG CTG CCC TCA GAG-3’; reverse: 5’-CAT CAA TTA GTA CAC AAA TTA CTG-3’). Two forward primers (25 μM each) and the reverse primer (50 μM) were used together to detect the *Stat3*$^{\Delta}$ allele.

For chemical-induction of hepatocarcinogenesis, mice at postnatal day 15 were injected intraperitoneally with diethylnitrosamine (25 mg/kg, Sigma Aldrich N0258-1G), and then weaned and maintained on regular chow food. Livers and tumors were pictured and harvested for analysis 8 months after the initial injection (He et al., 2010; Maeda et al., 2005). All animals were housed in virus-free facility and maintained in a temperature and light (12-hour light/dark cycle) controlled animal facility. Mice were permitted ad libitum access to water and standard chow. The SBMRI and UCSD Animal Use Committees approved all protocols.

Histology and immunostaining

Liver fixation in paraffin and H&E staining of 5 μm sections were performed using standard protocols. The same slides were subjected to Masson's trichrome staining (Poly Scientific) or reticulin staining that was performed according to Gordon-sweets reticulum procedure (Poly Scientific). TUNEL assay was conducted using ApopTag Plus Peroxidase In Situ Apoptosis Detection Kit (Chemicon), and slides were counterstained with methyl green. Liver histology was examined by light microscopy in a blinded fashion. The extent of infiltration in parenchyma by inflammatory cells was semi-quantitatively estimated by assigning a severity score (absent: 0; mild: 1; moderate: 2; pronounced: 3; severe: 4). This score was used to compare the liver damage and inflammation between control and *Shp2*$^{hep-/-}$ mice after LPS challenge.

Aged animals drank 5-bromo-2’-deoxyuridine (BrdU, 1 mg/ml, Sigma, 1% sucrose, Sigma), and 4 mice in each group were sacrificed after two weeks. Withdrawn livers were prepared for 5-μm cryosectioning and immunostaining. BrdU labeling and detection Kit I was used to stain incorporated BrdU, and Vectashield mounting medium with Dapi (Vector) was used to stain nuclei. BrdU-positive hepatocytes was enumerated under fluorescent microscopy and

calculated by randomly counting BrdU-stained nuclei per 100 $Dapi^+$ nuclei in a total of at 2,000 hepatocytes.

LPS or IL-6 stimulation

Male animals (2–3 month-old littermates) were used. For 5-min stimulation, a solution of LPS (1 mg/ml in PBS, Sigma) was injected into the vena cava at the dosage of 0.5 mg/25g body weight, and livers were harvested and quickly frozen in liquid nitrogen. For later time points, 1, 3, 14, and 24 hr, 14 days, the same solution of LPS was injected intraperitoneally at a 4 mg/100 g body weight. Sera were collected at indicated time points, and livers were harvested for biochemistry and histology. Under anesthesia with Avertin (0.015 ml/g body weight), either 50 µl saline or 5µg murine IL-6 (Peprotech Inc) in 50 µl saline were injected into portal vein, and livers were harvested and quickly frozen 5 min later.

Serological and biochemical analyses

Venous blood was collected by bleeding of the retro-orbital sinus. Serum was separated after clotting. IL-6 and TNFα serum levels were determined by mouse Biotrak ELISA systems (Amersham Biosciences). Alanine aminotransferase (ALT) and aspartate aminotransferase (AST) levels in serum were measured by Animal Care Program, Diagnostic Laboratory, University of California, San Diego. Other inflammatory cytokine amounts in serum were assessed using Beadlyte Mouse Multi-Cytokine Detection System Kit from Upstate or a Meso Scale Discovery Assay. ELISA on liver extracts was performed as described previously (Cripps et al., 2010). 0.12 g/ml of liver tissue was homogenized in sucrose buffer (0.25 M sucrose, 10 mM Tris pH7.4, protease inhibitor cocktail) and cleared by centrifugation (9300 g, 10 min).

Frozen tissue samples were processed as previously described (Bard-Chapeau et al., 2006). Home-made antibody against Shp2 was described previously (Feng et al., 1993). Antibodies to p-Erk1/2, p-Tyr^{705}Stat3, p-Ser^{727}Stat3, Stat3, p-Stat1, p38 MAPK, p-p38 MAPK, IκBα, pAkt, and Akt were obtained from Cell Signaling. Antibodies to Erk2, Stat1, p-Jnk1/2, Jnk1/2 were obtained from Santa Cruz. When needed, films were scanned and signals were quantified using ImageQuant software.

Human HCC

Human liver specimens were obtained from HCC patients who underwent hepatectomy or liver transplantation in Eastern Hepatobiliary Surgery Hospital, Shanghai, China. Collection of patient samples with informed consent to an established protocol and all experimental procedures were approved by the Research Ethics Committee of Eastern Hepatobiliary Surgery Hospital. Tissue sections and tissue microarrays were incubated with anti-Shp2 antibody (Cell Signaling Technology, Inc.) at 4°C overnight and then with horseradish peroxidase-conjugated secondary antibody at 37°C for 30 min. The sections were finally incubated with diaminoenzidine and counterstained with H&E for detection.

Statistical analysis

Data analysis was performed using a two-tails unpaired t-test. Values were expressed as mean ± SEM. * $p<0.05$; ** $p<0.01$; *** $p<0.001$.

Supplementary Material

Refer to Web version on PubMed Central for supplementary material.

Acknowledgments

We thank Dr. M. David, S.M. Griffey, and M. Karin for invaluable advice and suggestion, and G. He, R. Tawatao, and N. Droin for technical assistance. This work was supported by grants from NIH (R01DK73945, R01DK75916), and State key program of liver cancer (2008ZX10002) from NNSF of China 30921006.

REFERENCES

1. Alonzi T, Maritano D, Gorgoni B, Rizzuto G, Libert C, Poli V. Essential role of STAT3 in the control of the acute-phase response as revealed by inducible gene inactivation [correction of activation] in the liver. Mol Cell Biol. 2001; 21:1621–1632. [PubMed: 11238899]
2. Bard-Chapeau EA, Yuan J, Droin N, Long S, Zhang EE, Nguyen TV, Feng GS. Concerted functions of Gab1 and Shp2 in liver regeneration and hepatoprotection. Mol Cell Biol. 2006; 26:4664–4674. [PubMed: 16738330]
3. Bishop JM. Molecular themes in oncogenesis. Cell. 1991; 64:235–248. [PubMed: 1988146]
4. Blume-Jensen P, Hunter T. Oncogenic kinase signalling. Nature. 2001; 411:355–365. [PubMed: 11357143]
5. Chan RJ, Feng GS. PTPN11 is the first identified proto-oncogene that encodes a tyrosine phosphatase. Blood. 2007; 109:862–867. [PubMed: 17053061]
6. Chan RJ, Johnson SA, Li Y, Yoder MC, Feng GS. A definitive role of Shp-2 tyrosine phosphatase in mediating embryonic stem cell differentiation and hematopoiesis. Blood. 2003; 102:2074–2080. [PubMed: 12791646]
7. Coussens LM, Werb Z. Inflammation and cancer. Nature. 2002; 420:860–867. [PubMed: 12490959]
8. Cripps JG, Wang J, Maria A, Blumenthal I, Gorham JD. Type 1 T helper cells induce the accumulation of myeloid-derived suppressor cells in the inflamed Tgfb1 knockout mouse liver. Hepatology. 2010; 52:1350–1359. [PubMed: 20803559]
9. Feng GS, Hui CC, Pawson T. SH2-containing phosphotyrosine phosphatase as a target of protein-tyrosine kinases. Science. 1993; 259:1607–1611. [PubMed: 8096088]
10. Greten FR, Eckmann L, Greten TF, Park JM, Li ZW, Egan LJ, Kagnoff MF, Karin M. IKKbeta links inflammation and tumorigenesis in a mouse model of colitis-associated cancer. Cell. 2004; 118:285–296. [PubMed: 15294155]
11. He G, Yu GY, Temkin V, Ogata H, Kuntzen C, Sakurai T, Sieghart W, Peck-Radosavljevic M, Leffert HL, Karin M. Hepatocyte IKKbeta/NF-kappaB inhibits tumor promotion and progression by preventing oxidative stress-driven STAT3 activation. Cancer Cell. 2010; 17:286–297. [PubMed: 20227042]
12. Lai, LA.; Zhao, C.; Zhang, EE.; Feng, GS. The Shp-2 tyrosine phosphatase. In: Arino, J.; Alexander, D., editors. Protein phosphatases. Berlin Heidelberg: Springer-Verlag; 2004. p. 275-299.
13. Levine AJ, Puzio-Kuter AM. The control of the metabolic switch in cancers by oncogenes and tumor suppressor genes. Science. 2010; 330:1340–1344. [PubMed: 21127244]
14. Luedde T, Beraza N, Kotsikoris V, van Loo G, Nenci A, De Vos R, Roskams T, Trautwein C, Pasparakis M. Deletion of NEMO/IKKgamma in liver parenchymal cells causes steatohepatitis and hepatocellular carcinoma. Cancer Cell. 2007; 11:119–132. [PubMed: 17292824]
15. Maeda S, Kamata H, Luo JL, Leffert H, Karin M. IKKbeta couples hepatocyte death to cytokine-driven compensatory proliferation that promotes chemical hepatocarcinogenesis. Cell. 2005; 121:977–990. [PubMed: 15989949]
16. Neel BG, Gu H, Pao L. The 'Shp'ing news: SH2 domain-containing tyrosine phosphatases in cell signaling. Trends Biochem Sci. 2003; 28:284–293. [PubMed: 12826400]
17. Revillion F, Puech C, Rabenoelina F, Chalbos D, Peyrat JP, Freiss G. Expression of the putative tumor suppressor gene PTPN13/PTPL1 is an independent prognostic marker for overall survival in breast cancer. Int J Cancer. 2009; 124:638–643. [PubMed: 19004008]
18. Sefton BM, Hunter T. From c-src to v-src, or the case of the missing C terminus. Cancer Surv. 1986; 5:159–172. [PubMed: 2430701]

19. Servidei T, Aoki Y, Lewis SE, Symes A, Fink JS, Reeves SA. Coordinate regulation of STAT signaling and c-fos expression by the tyrosine phosphatase SHP-2. J Biol Chem. 1998; 273:6233–6241. [PubMed: 9497348]
20. Sun T, Aceto N, Meerbrey KL, Kessler JD, Zhou C, Migliaccio I, Nguyen DX, Pavlova NN, Botero M, Huang J, et al. Activation of Multiple Proto-oncogenic Tyrosine Kinases in Breast Cancer via Loss of the PTPN12 Phosphatase. Cell. 2011; 144:703–718. [PubMed: 21376233]
21. Tartaglia M, Gelb BD. Germ-line and somatic PTPN11 mutations in human disease. Eur J Med Genet. 2005; 48:81–96. [PubMed: 16053901]
22. Tartaglia M, Martinelli S, Stella L, Bocchinfuso G, Flex E, Cordeddu V, Zampino G, Burgt I, Palleschi A, Petrucci TC, et al. Diversity and Functional Consequences of Germline and Somatic PTPN11 Mutations in Human Disease. Am J Hum Genet. 2006; 78:279–290. [PubMed: 16358218]
23. Tartaglia M, Niemeyer CM, Fragale A, Song X, Buechner J, Jung A, Hahlen K, Hasle H, Licht JD, Gelb BD. Somatic mutations in PTPN11 in juvenile myelomonocytic leukemia, myelodysplastic syndromes and acute myeloid leukemia. Nat Genet. 2003; 34:148–150. [PubMed: 12717436]
24. Veeriah S, Brennan C, Meng S, Singh B, Fagin JA, Solit DB, Paty PB, Rohle D, Vivanco I, Chmielecki J, et al. The tyrosine phosphatase PTPRD is a tumor suppressor that is frequently inactivated and mutated in glioblastoma and other human cancers. Proc Natl Acad Sci U S A. 2009; 106:9435–9440. [PubMed: 19478061]
25. Wang Z, Shen D, Parsons DW, Bardelli A, Sager J, Szabo S, Ptak J, Silliman N, Peters BA, van der Heijden MS, et al. Mutational analysis of the tyrosine phosphatome in colorectal cancers. Science. 2004; 304:1164–1166. [PubMed: 15155950]
26. Weinberg RA. The molecular basis of oncogenes and tumor suppressor genes. Ann N Y Acad Sci. 1995; 758:331–338. [PubMed: 7625701]
27. Wu D, Pang Y, Ke Y, Yu J, He Z, Tautz L, Mustelin T, Ding S, Huang Z, Feng GS. A conserved mechanism for control of human and mouse embryonic stem cell pluripotency and differentiation by shp2 tyrosine phosphatase. PLoS ONE. 2009; 4:e4914. [PubMed: 19290061]
28. Xu R, Yu Y, Zheng S, Zhao X, Dong Q, He Z, Liang Y, Lu Q, Fang Y, Gan X, et al. Overexpression of Shp2 tyrosine phosphatase is implicated in leukemogenesis in adult human leukemia. Blood. 2005; 106:3142–3149. [PubMed: 16030196]
29. You M, Yu DH, Feng GS. Shp-2 tyrosine phosphatase functions as a negative regulator in the interferon-stimulated Jak/STAT pathway. Mol Cell Biol. 1999; 19:2416–2424. [PubMed: 10022928]
30. Yu H, Kortylewski M, Pardoll D. Crosstalk between cancer and immune cells: role of STAT3 in the tumour microenvironment. Nat Rev Immunol. 2007; 7:41–51. [PubMed: 17186030]
31. Yu H, Pardoll D, Jove R. STATs in cancer inflammation and immunity: a leading role for STAT3. Nat Rev Cancer. 2009; 9:798–809. [PubMed: 19851315]
32. Zhang EE, Chapeau E, Hagihara K, Feng GS. Neuronal Shp2 tyrosine phosphatase controls energy balance and metabolism. Proc Natl Acad Sci U S A. 2004; 101:16064–16069. [PubMed: 15520383]
33. Zhou X, Coad J, Ducatman B, Agazie YM. SHP2 is up-regulated in breast cancer cells and in infiltrating ductal carcinoma of the breast, implying its involvement in breast oncogenesis. Histopathology. 2008; 53:389–402. [PubMed: 18643929]

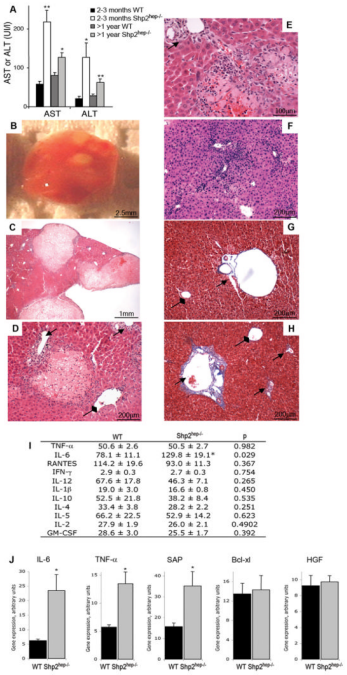

	WT	$Shp2^{hep-/-}$	p
TNF-α	50.6 ± 2.6	50.5 ± 2.7	0.982
IL-6	78.1 ± 11.1	129.8 ± 19.1*	0.029
RANTES	114.2 ± 19.6	93.0 ± 11.3	0.367
IFN-γ	2.9 ± 0.3	2.7 ± 0.3	0.754
IL-12	67.6 ± 17.8	46.3 ± 7.1	0.265
IL-1β	19.0 ± 3.0	16.6 ± 0.8	0.450
IL-10	52.5 ± 21.8	38.2 ± 8.4	0.535
IL-4	33.4 ± 3.8	28.2 ± 2.2	0.251
IL-5	66.2 ± 22.5	52.9 ± 14.2	0.623
IL-2	27.9 ± 1.9	26.0 ± 2.1	0.4902
GM-CSF	28.6 ± 3.0	25.5 ± 1.7	0.392

Figure 1. Hepatic damage and inflammation in *Shp2*$^{hep-/-}$ mice

(A) Circulating blood levels of AST and ALT were quantified in control or *Shp2*$^{hep-/-}$ mice at indicated ages; n = 4–8, * p<0.05; ** p<0.01 for *WT* versus *Shp2*$^{hep-/-}$.

(**B**) Gross appearance of the right lobe of a *Shp2*$^{hep-/-}$ liver showing pale acellular regions.

(**C**) H&E staining of a *Shp2*$^{hep-/-}$ liver section showed inflammation and macroscopic necrosis.

(**D**) H&E staining showed a small necrotic area surrounded and infiltrated by inflammatory cells in *Shp2*$^{hep-/-}$ liver section. In D–H, Arrows indicate portal triads and diamond arrow shows central vein.

(**E**) A necrosis area was surrounded by inflammatory infiltrates in H&E stained *Shp2*$^{hep-/-}$ liver section.

(**F**) H&E staining showed severe inflammatory infiltrates in *Shp2*$^{hep-/-}$ liver.

(**G–H**) Trichrome staining showed low and high levels of collagen secret surrounding the portal triad of control (G) and *Shp2*$^{hep-/-}$ (H) liver sections, respectively.

(**I**) Circulating blood levels of inflammatory cytokines were quantified at 2–3 months of age (n = 7–18, * p<0.05).

(J) Hepatic gene expression of *IL-6, TNF, Bcl-xl* and *HGF* was assessed by qRT-PCR of total mRNAs isolated from 2–3-month-old mouse livers. The results were average of 3 mice, and absolute mRNA values were determined and normalized to cyclophilin.

See also Figure S1.

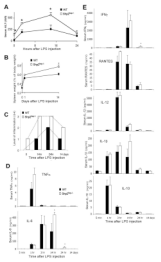

Figure 2. Hypersensitivity to LPS in *Shp2*$^{hep-/-}$ animals

(A) Circulating blood levels of ALT were quantified in *WT* and *Shp2*$^{hep-/-}$ mice at indicated time points after LPS injection (n = 3–4).

(B) Spleen weight was measured and normalized to body weight at several time points after LPS challenge (n = 5).

(C) Graphic representation of hepatic inflammation levels. Values from 0 to 4 were given to each H&E slide according to the level of infiltration by inflammatory cells. An average was calculated from 5–10 mice of each genotype.

(D) Circulating serum levels of TNFα and IL-6 were determined at indicated time points after LPS injection (n = 3–7, * $p<0.05$ for *WT* versus *Shp2*$^{hep-/-}$).

(E) Serum levels of IFNγ, RANTES, IL-12, IL-1β and IL-10 were quantified at indicated time points after LPS administration (n = 3–7).

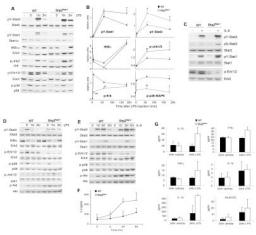

Figure 3. Altered hepatic LPS and IL-6 signaling events in vivo and in vitro

(A) Mice were injected with LPS, and pY-Stat1, pY-Stat3, p-Jnk1/2, p-Erk1/2, and p-p38 MAPK were assessed by immnoblotting with their protein levels as controls. IκBα degradation was assessed, using Erk2 protein as control.

(B) The phospho-signals were quantified and normalized against total liver protein amounts. IκBα protein amounts were normalized against Erk2 The relative signal levels were determined by setting the value of the control at 1 hr as 1 unit. (n = 3–6, * $p<0.05$, ** $p<0.01$ for *WT* versus $Shp2^{hep-/-}$).

(C) Immunoblotting of liver lysates was performed 5 min after injection of IL-6 (5 μg) into portal vein. pY-Stat3 and pS-Stat3, and p-Erk levels were assessed.

(D, E) pY-Stat3 and pS-Stat3, p-Jnk1/2, p-Akt (Ser473), p-Erk, p-and p38 MAPK were assessed by immunoblot analysis with protein levels as control. The IκBα degradation was compared to Erk2 protein level.

(F–G) Amounts of inflammatory cytokines were quantified in supernatants from *WT* and $Shp2^{hep-/-}$ hepatocytes (n = 3).

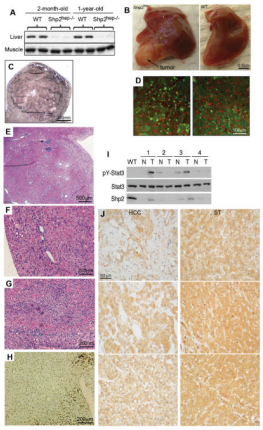

Figure 4. Spontaneous development of hepatocellular adenoma in aged *Shp2*$^{hep-/-}$ mice

(A) Immunoblot analysis of Shp2 protein levels in the liver and muscle isolated from young or old *WT* and *Shp2*$^{hep-/-}$ mice.

(B) Macroscopic view of hepatic adenomas that bulged from the surface of *Shp2*$^{hep-/-}$ liver and appeared pale compared to the hepatic parenchyma.

(C) Reticulin staining of an adenoma.

(D) Hepatocyte proliferation in *Shp2*$^{hep-/-}$ (left panel) and *WT* (right panel) aged littermate mice. BrdU-positive cells were shown green, Dapi stained nuclei were red.

(E) H&E staining of an adenoma. Arrowhead points to a focal granuloma.

(F) H&E staining showed nodular regenerative hyperplasia.

(G) H&E staining showed hepatocyte degeneration, associated with vacuoles containing eosinophilic material at the periphery of adenoma.

(H) TUNEL assay revealed an area of focal apoptosis (dark brown nuclei) in the liver parenchyma. Slides were counterstained with methylgreen.

(I) pY-Stat3 levels in WT, tumoral *Shp2*$^{hep-/-}$ parenchyma (T) and non-tumoral (N) parenchyma of 18-month-old mice, as assessed by immunoblotting of tissue extracts.

(J) Human HCC specimens and corresponding surrounding tissue (ST) from the same patient were immunostained for Shp2. Shown here are 3 representative samples with Shp2 contents lower in HCC than in ST.

See also Figure S2.

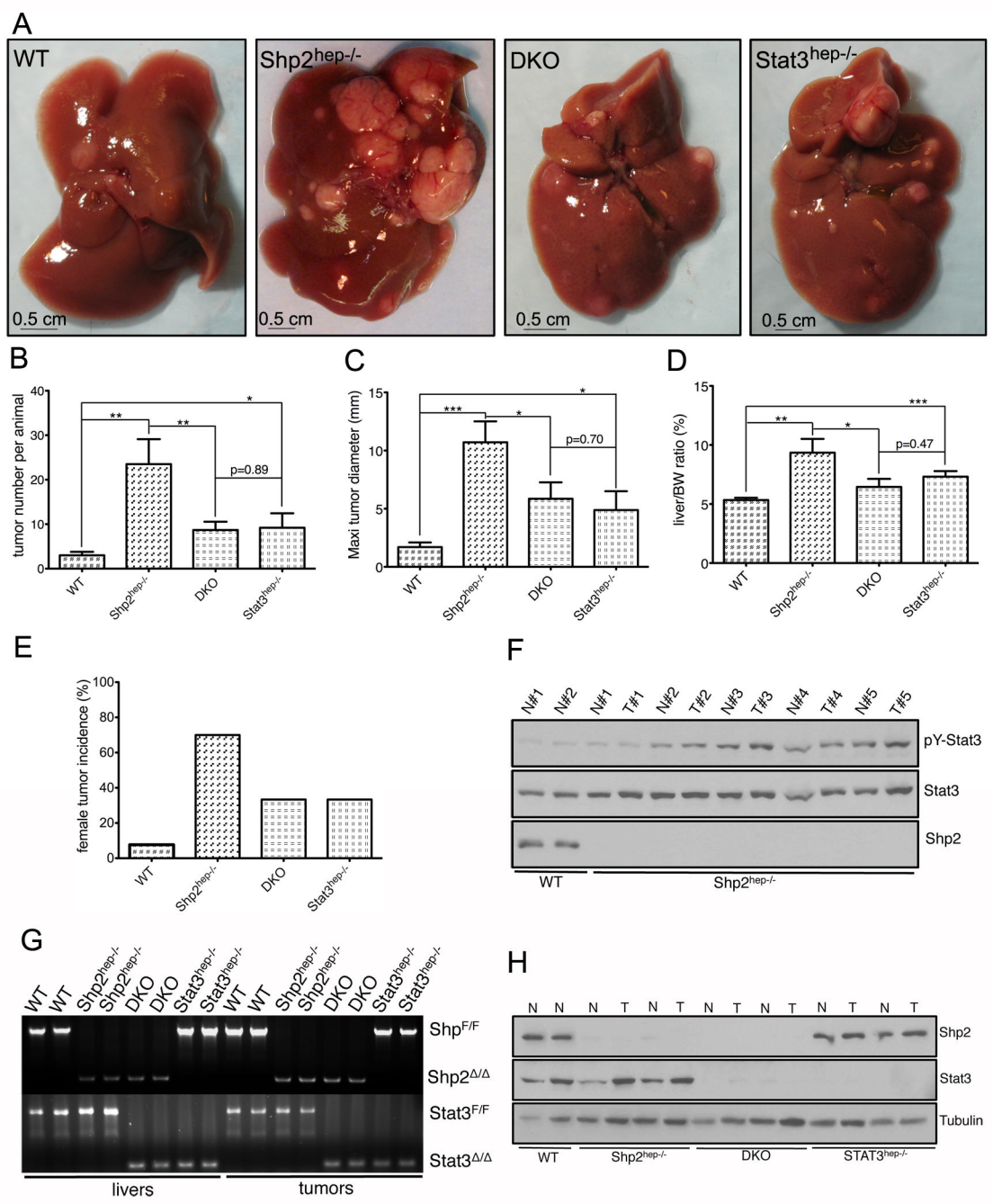

Figure 5. Enhanced HCC development in *Shp2*$^{hep-/-}$ livers is compromised by additional deletion of Stat3

(A) Gross appearances of representative livers with tumors in control (*WT*), *Shp2*$^{hep-/-}$, *Shp2/Stat3*$^{hep-/-}$ (*DKO*), and *Stat3*$^{hep-/-}$ male mice.

(B) Liver tumor numbers were compared between WT, *Shp2*$^{hep-/-}$, *Stat3*$^{hep-/-}$ and DKO mice (male, n = 5–13).

(C) Average maximal diameters of tumors were measured and compared between *WT*, *Shp2*$^{hep-/-}$, *Stat3*$^{hep-/-}$ and *DKO* livers (male, n = 5–13).

(D) The liver/body weight ratios were determined and compared between the four groups of mice (male, n = 5–13).

(E) Tumor incidences were determined in *WT*, *Shp2*$^{hep-/-}$, *Stat3*$^{hep-/-}$, and *DKO* female mice (n = 6–13).
(F) Immunoblotting was performed to evaluate pY-Stat3 levels in tumors (T) and surrounding hepatic tissues (N).
(G) Deletion of Shp2 and/or Stat3 in *Shp2*$^{hep-/-}$, *Stat3*$^{hep-/-}$ or DKO livers was evaluated by PCR analysis of genomic DNA extracted from tumor or surrounding liver tissues.
(H) Immunoblotting was performed for protein extracts from tumor (T) and surrounding liver tissues (N), to determine Shp2 and/or Stat3 removal.

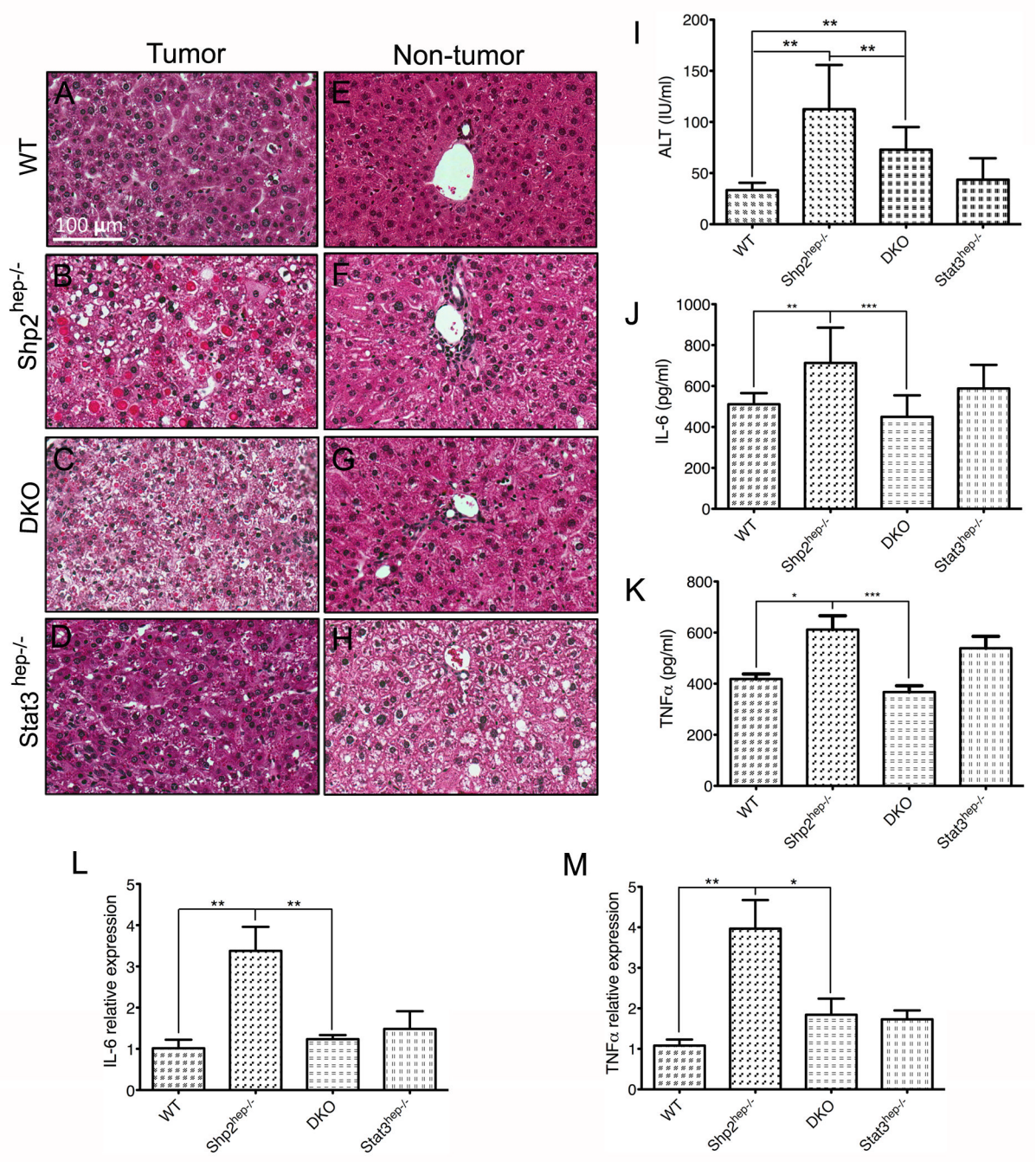

Figure 6. Increased inflammation in *Shp2*$^{hep-/-}$ livers is reduced by combined deletion of Shp2 and Stat3

(A–D) Representative H&E staining of tumor samples showed typical trabecular structures in control and *Stat3*$^{hep-/-}$ livers, but not in *Shp2*$^{hep-/-}$ and DKO livers, and reduced size of eosinophilic vacuoles of degeneration in DKO liver.

(E–H) Representative H&E staining of liver samples showed infiltrate of inflammatory cells in portal triads of *Shp2*$^{hep-/-}$ and DKO livers, and fat droplets in *Stat3*$^{hep-/-}$ liver.

(I) Serum ALT levels were measured in the four groups of mice.

(J–K) IL-6 and TNFα levels in liver extracts were measured by ELISA.

(L–M) qRT-PCR was performed to determine *IL-6* and *TNFα* mRNA levels.

(I–M: n = 5–11; * $p<0.05$; ** $p<0.01$; *** $p<0.001$).